Cement and Concrete Research xxx (xxxx) xxx–xxx

Contents lists available at ScienceDirect

Cement and Concrete Research

journal homepage: www.elsevier.com/locate/cemconres

Role of alcohol-ethylene oxide polymers on the reduction of shrinkage of cement paste

Ippei Maruyama[a,*], Ellis Gartner[b], Katsutoshi Beppu[a], Ryo Kurihara[a]

[a] Graduate School of Environmental Studies, Nagoya University, Japan
[b] Department of Civil and Environmental Engineering, Imperial College, London SW7 2AZ, UK

ARTICLE INFO

Keywords:
Shrinkage (C)
C-S-H (B)
Admixture (D)
Shrinkage-reducing agent

ABSTRACT

Concrete drying shrinkage is a major practical problem, but it can be ameliorated by means of "shrinkage-reducing agents" (SRAs). Water vapor sorption isotherms and low temperature DSC measurements suggest that alcohol-ethylene oxide polymers (AEOPs) with a better hydrophilic-lipophilic (HL-) balance are present in meso-pores in which water molecules evaporate from 75% RH to 40% RH. Short-term drying shrinkage measurements show that the better HL-balanced AEOPs reduce irreversible shrinkage, which occurs mainly from 75% RH to 40% RH during the first drying. Based on the similarity between corresponding RH regions, it is concluded that the better HL balanced AEOP in relevant meso-pores hinders agglomeration of C-S-H during the first desorption to mitigate the irreversible shrinkage and reduce the first drying shrinkage.

1. Introduction

Shrinkage reducing agents (SRAs) are admixtures, first developed in Japan [1], that are used to reduce the drying shrinkage and cracking of concrete. Shrinkage-induced cracking is unsightly and can also reduce concrete durability by various mechanisms, e.g. by allowing intrusion of chloride ions and carbon dioxide gas, which promote steel corrosion in reinforced concrete. SRAs are often used to mitigate cracking, but the mechanism of shrinkage reduction is still poorly understood.

The first generation of SRAs were moderately water-soluble non-ionic organic solutes known to reduce the surface tension of water [2]. However, it was noted that it was usually necessary to use them at aqueous concentrations well above their apparent "critical micelle concentration" (CMC) in order to obtain the maximum effect on reducing free drying shrinkage of hardened cement pastes (hcp) [3,4]. These experimental results threw doubt on the idea that SRAs work solely via a capillary tension mechanism [5]; despite intensive additional research [5–12], their mechanism remains poorly understood. Recently, we showed that SRAs reduce the unrestrained drying shrinkage of hcp mainly during the first desorption, but have little impact on further length changes during rewetting and further drying after sufficiently long process times for altering the calcium silicate hydrate (C-S-H)[1] [13]. In cases of short term drying and wetting cycles of the mortar with lower water to cement ratio, the continuous impact was confirmed to show contrary behavior [12]. The difference might be explained by a difference of drying period for C-S-H and a difference in amount of outer C-S-H which has large impact on the irreversible shrinkage. It was also shown that portlandite crystals in hcp can be strongly modified by the use of certain SRAs [7,12,13], which seems consistent with observations that simple alcohols modify the morphology and increase the specific surface area of portlandite produced by slaking quicklime, apparently by preferential adsorption on the 001 crystal face, where alkoxide (-OR) groups can partially replace hydroxide (-OH) groups [14,15]. It is thus conceivable that certain SRAs might also modify the nanostructure of calcium silicate hydrate (C-S-H), possibly by interaction with some of its –OH groups [16]. C-S-H is a highly basic solid-solution phase of widely-varying composition, thought to be composed mainly of tobermorite-like anionic basal layers, with associated calcium cations for charge balance [17–19]. The C-S-H produced during cement or C_3S hydration is formed at a high pH from solutions slightly supersaturated with respect to portlandite. It has a very disordered structure [20,21] with many Ca-OH groups [16], which could be partly alkylated to give some Ca-OR groups.

Based on many such prior studies, a new model for the structure of the "wet" C-S-H initially formed in Portland cement hydration was recently proposed by Gartner et al. [22]. We will refer to it here as the "GMC" model. In this model, freshly-precipitated C-S-H is composed of tobermorite-like basal layers containing primarily dimeric silicate anions bonded to both sides of basal CaO sheets. The negative charge of the simplest basal sheet repeating unit, ($[Ca_2Si_2O_7]^{2-}$), is initially

* Corresponding author.
E-mail addresses: ippei@dali.nuac.nagoya-u.ac.jp (I. Maruyama), e.gartner@imperial.ac.uk (E. Gartner), r-kurihara@dali.nuac.nagoya-u.ac.jp (R. Kurihara).

[1] Oxide notation is used for cement compounds: C = CaO; S = SiO_2; H = H_2O; A = Al_2O_3; F = Fe_2O_3; and R represents an alkyl group.

https://doi.org/10.1016/j.cemconres.2018.05.017
Received 9 July 2017; Received in revised form 17 April 2018; Accepted 24 May 2018

balanced by fully-hydrated calcium cations, either divalent (Ca^{2+}) or univalent ($CaOH^{+}$), and it is assumed that each such cation holds at least 6 oxygen atoms in their inner coordination shell. Thus, fresh wet C-S-H can be represented as a solid solution between the end members ($[Ca_2Si_2O_7]^{2-}\cdot[Ca(H_2O)_6]^{2+}$) (= $C_3S_2H_6$) and ($[Ca_2Si_2O_7]^{2-}\cdot 2[Ca(OH)(H_2O)_5]^{+}$) (= $C_4S_2H_{11}$). If γ represents the fraction of the low Ca/Si end members of this solid solution, it can readily be seen that for $\gamma = 0.4$, the composition of the solid solution becomes $C_{1.7}SH_4$. This composition is the same as that assumed by Young and Hansen [23] to account for the minimum amount of water required for complete cement hydration.

In the GMC paper [23], it is hypothesized that the organic molecules used as SRAs have a tendency to adsorb weakly onto C-S-H basal surfaces, partially shielding the silicate groups and thus inhibiting their reaction with initially hydrated charge-balancing calcium ions, while there are unsuccessful attempts to measure adsorption of non-ionic surfactants on C-S-H [24–26]. This prevents formation of calcium bridges between silicate groups brought into close proximity by capillary forces during drying. However, the roles of the different structural elements in SRA molecules are not yet well understood. In the present work, a set of 15 alcohol-ethylene oxide polymers (AEOPs) was obtained by varying the two main molecular structural elements: alcohol (alkyl group) type and poly-EO chain length. The relative effects of these changes on the hygral equilibria and drying shrinkage of hcp was then studied with the objective of determining the relationship between molecular structure and SRA performance.

2. Experimental method

2.1. Materials

We used a white cement provided by Taiheiyo Cement Corporation, the same as that used in two previous papers [27,28]. Its density was 3.05 g/cm^3, and its Blaine specific surface area was 349 m^2/kg. The chemical composition, and the mineralogical composition determined by a powder X-ray diffraction (XRD)/Rietveld method, are shown in Table 1 and Table 2, respectively.

The 15 AEOP molecules used in this work, shown in Table 3, were synthesized by Dr. Akihiro Furuta of Takemoto Oil & Fat Co. Ltd., Japan. They were derived either from water (C0(=H)) or 3 different aliphatic alcohols: ethanol (C2), butanol (C4), and 2-ethylhexanol (C8). The number of polymerized ethylene oxide (EO) units per molecule was 0 (for the simple alcohols), 2, 20, or 100. The surface tension of AEOP solutions whose concentration is equivalent to the initial mixed condition was measured using the Wilhelmy method. The results are summarized in Fig. 1.

Cement paste samples were made from white cement and de-ionized water, with 2% added AEOP by mass of cement replacing water, such that the (water + AEOP)/cement ratio was 0.55 by mass. The densities of the various AEOPs are different; therefore, the theoretical volumetric ratios of liquids to solids were different. However, a 3.46 mass% AEOP concentration solution is almost 1.0 g/cm^3, and the initial spaces between cement particles could be comparable. There is a possibility that the degree of hydration will be affected by this difference of available space for precipitation due to the presence of AEOP molecules. The experimental results will be discussed with respect to phase composition. For AEOPs with 20 or more EO groups, excessive volumes of air were entrained during standard mixing, so a vacuum mixer (Renfert Vacuum mixer twister II) was used. A 400 mL sample of cement paste was mixed for 1 min, scraped from inside the mixer, and then followed by remixing for a further 3 min. To minimize segregation, the paste was remixed manually every 30 min up to 6 h, after which it had a creamy consistency. It was then cast into a set of 3 × 13 × 300 mm slab molds, which were covered by wet paper and a poly-vinylidene-dichloride film wrap to avoid water loss from the specimens. The covered molds were stored in a thermostatic chamber at 20 ± 1 °C. The slabs were demolded after 4 days, cut into 100 mm lengths with a precision cutting machine, and then immediately stored in aluminized polymer bags for 28 days after mixing. The samples were cut using water cooling to avoid a heat impact on the samples. Due to the usage of water cooling, some of the SRA can be washed out of the sample; however, this region is only 1–2 mm from both edges, which does not have a significant impact on length change measurements. After this initial curing regime, the samples were dried for 8 weeks at 60% RH. Further details of this procedure are given in the section on long-term drying experiments.

2.2. Measurements

The phase compositions of cement paste samples were determined by XRD/Rietveld analysis. Samples sealed for 28 days, which corresponds to the beginning of drying, were submerged in acetone for 6 h, and then dried under vacuum for several minutes with an aspirator. The specimens were then stored over a saturated LiCl solution at 20 ± 2 °C for 2 weeks. The protocol for the XRD/Rietveld analysis are the same as those described in ref. [27,29]. Three samples were measured for each condition.

Thermogravimetric analyses were conducted on ~20 mg samples from the 28-day sealed samples. Dynamic TG measurements were conducted under N_2 gas flow from room temperature to 1000 °C, including a 7-hour holding period at 105 °C. The mass change from the end of the 7-hour 105 °C holding period up to 550 °C is referred to here as “chemically bound” water, and the mass change from room temperature to the end of the 7-hour 105 °C holding period is referred to here as “evaporable water.” Evaporable water was referenced to the mass of the sample at the end of the 7-hour 105 °C holding period, and chemically bound water was referenced to the mass after heating to 550 °C. Other types of thermogravimetric analysis were conducted to show differential thermal gravimetry (DTG) for sealed samples at 28 days. A measurement was taken under N_2 gas flow with a 10 °C/min temperature ramp, and this method was applied to the sample at 28 days.

Water vapor sorption isotherm (WVSI) measurements were conducted by the volume method (or manometric method) using a water vapor sorption analyzer (Hydrosorb 1000, Quantachrome). The samples were ground in a ball mill, and ~20 mg samples of powder with a particle size in the range of 25–75 μm were used for the analysis. The particles were extracted using sieves with 25 μm and 75 μm openings. The parameters of the measurements were a pressure tolerance of 0.05 mm Hg and a time tolerance of 120 s. The measurement points on the adsorption and desorption branches were at $p/p_0 = 0.05$ intervals up to 0.95 and ended at 0.98 (RH = 98%). For pre-treatment, the

Table 1
Chemical composition of white cement by X-ray fluorescence elemental analysis[a].

LOI (%)	Chemical composition (mass%)											
	SiO_2	Al_2O_3	Fe_2O_3	CaO	MgO	SO_3	Na_2O	K_2O	Ti O_2	P_2O_5	MnO	Cl^-
2.93	22.43	4.67	0.16	65.69	0.98	2.51	0.00	0.07	0.17	0.03	0.00	0.00

[a] Conducted by Taiheiyo Cement Corporation.

Table 2
Mineral composition of white cement determined by a powder XRD/Rietveld analysis.

Alite	Belite	Aluminate	Periclase	Bassanite	Gypsum	Calcite
53.1 ± 1.4	33.2 ± 1.5	5.46 ± 0.37	0.5 ± 0.27	2.01 ± 0.23	1.84 ± 0.11	3.96 ± 0.7

Table 3
Synthesized alcohol-ethylene oxide polymers (AEOPs) and the notations used to describe the cement pastes made with these polymers. (PL = plain paste).

Base "alcohol" group	Number of EO groups			
	0	2	20	100
Water (C0) = (H)	PL	C0(H)-EO-2	C0(H)-EO-20	C0(H)-EO-100
Ethanol (C2)	C2-EO-0	C2-EO-2	C2-EO-20	C2-EO-100
Butanol (C4)	C4-EO-0	C4-EO-2	C4-EO-20	C4-EO-100
2-Ethylhexanol (C8)	C8-EO-0	C8-EO-2	C8-EO-20	C8-EO-100

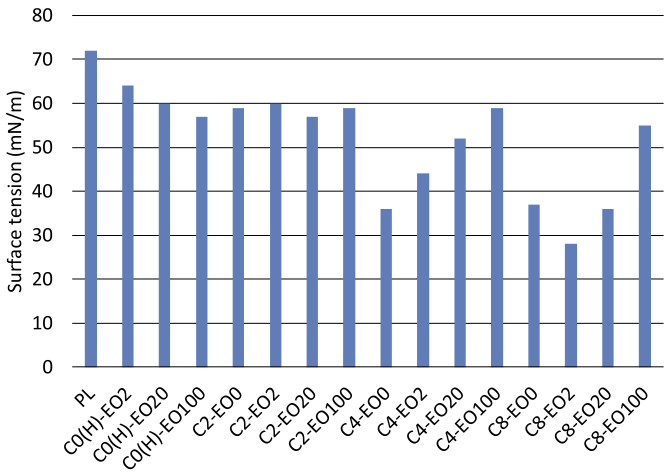

Fig. 1. Surface tensions of 3.64% AEOP solutions.

Table 4
Temperature—time profile use in DSC measurements.

Step	Temperature range	Rate of temperature change
1	Room temperature to 15 °C	± 10 °C/h
2	15 °C	5 min hold
3	15 to −60 °C	−10 °C/h
4	−60 °C	10 min hold

samples were dried under vacuum for 30 min (using a vacuum pump with a theoretical minimum pressure of 6.7×10^{-2} Pa and an observed maximum pressure of 60 Pa by the end of the drying process) while heating them with a heating mantle to maintain them at 105 °C; this led to the very dry initial state positioned for convenience at "0% RH" on the sorption isotherm graphs.

Low-temperature calorimetry (LTC) was run on all samples by differential scanning calorimetry (DSC, DSC3100SA (BrukerAXS)). Fragments of about 10 mg mass were obtained by crushing 3 × 13 × 100 mm specimens of the cured hcp samples with a hammer. They were submerged (initially under vacuum) in pure water for 5 min. Then, the surface water was removed by wiping the fragments with a bonded textile to give a saturated surface-dry (SSD) condition (Note: since the AEOP molecules have surfactant properties, they could have influenced the amount of water transferred to the textile and thus the amount of water retained under SSD conditions. But the bulk density of the hcp samples as obtained by the Archimedes method, the water absorption at saturation, and the degree of hydration of cement did not show significant differences among the samples). The SSD samples were used for the LTC measurements, following the temperature-time profile shown in Table 4. The reference sample for the measurement was corundum with a mass equal to the samples.

For the long-term drying experiment, the length and mass of 3 × 13 × 100 mm slab samples were measured using a mass balance (with a precision of 0.001 mg) and a displacement meter (with a precision of 1 μm). The initial condition for the samples was the sealed condition, and all samples were dried at 60% RH and 20 ± 2 °C for 8 weeks. For the length measurement, a 100 mm reference sample made from invar steel was used, and the difference in length was measured before and after drying. Shrinkage strain was calculated by dividing shrinkage deformation by the original length. Five specimens were used for each condition, and the average and standard deviation were calculated from the results.

For short-term drying experiments, length-change isotherms for samples were obtained with a thermomechanical analyzer (TMA) coupled with a RH generator (TMA4000SA and HC9700, Bruker AXS). Length changes were measured with a linear variable differential transformer (LVDT) with a resolution of 0.0025 μm and a contact load of 0.098 N. Samples 3 × 3 × 1 mm in size were cut from slab specimens for a more rapid experimental technique in which these very small specimens were subjected to forced drying under an RH-controlled air flow. Samples, which were never dried, were submerged in saturated limewater (initially under vacuum) for 5 min., then incrementally dried from 90% RH to 10% RH, after which they were incrementally re-humidified back up to 90% RH. All of these processes were conducted at 20 ± 0.1 °C. For each step, the RH of the atmospheric flow was kept constant for 8 h.

3. Experimental results

3.1. Specimen characterization

The phase compositions of the cement pastes cured for 28 days under sealed conditions are shown in Table 5. Degrees of hydration of alite and belite are plotted in Fig. 2. Cement pastes containing AEOPs showed lower degrees of hydration of alite and belite than the plain "control" paste, (PL), except for the paste C0(H)-EO2-2 (i.e. with diethylene glycol (DEG)), which showed a slightly greater degree of hydration. The aluminate phase (C_3A) was fully hydrated in all cases. The reduction in the degree of hydration of the silicate phases might be explained by the reduction of the actual water to cement ratio in the samples. However, the amounts of amorphous phase and portlandite were almost identical for all cement paste samples except for the sample with DEG. Based on these experimental data, direct comparisons of physical properties seem justifiable. In the case of the paste containing DEG, cement hydration was enhanced, but the formation of crystalline CH was repressed, while the amount of amorphous phase increased dramatically to compensate (Fig. 3). It should be noted that in the DEG case, tobermorite was found. Therefore, hcp containing DEG seems to be an anomaly. All of the XRD charts are shown in supporting material.

Chemically bound water and evaporable water were determined by dynamic TG measurements. The results are summarized in Fig. 4. As shown in the DTG curves in Fig. 5, slight carbonation was observed in samples containing AEOP. A similar trend is observed with samples containing isopropanol, acetone, methanol, and ethanol [30–32]. This is explained by the CO_2 produced by the oxidation of organic carbons in

Table 5
Phase composition of sealed-cured cement pastes at 28 days (mass %).

	Alite	Belite	Calcite	Ettrinngite	Monocarbonate	Hemicarbonate	Hydrogarnet	Portlandite	Tobermorite	Amorphous
Plain	3.25 ± 0.09	9.97 ± 0.31	2.07 ± 0.17	2.59 ± 0.13	6.05 ± 0.2	0.93 ± 0.08	1.39 ± 0.18	12.88 ± 0.1		60.87 ± 0.72
C0(H)-EO2	1.99 ± 0.19	8.11 ± 0.22	0.52 ± 0.17	8.81 ± 0.33	6.94 ± 0.24	1.03 ± 0.07	0.91 ± 0.15	3.25 ± 0.16	2.99 ± 0.2	65.45 ± 1.06
C0(H)-EO20	3.54 ± 0.32	11.01 ± 0.45	3.62 ± 0.24	3.65 ± 0.13	7.43 ± 0.33	0.8 ± 0.08	1.47 ± 0.2	12.25 ± 0.11		56.23 ± 0.94
C0(H)-EO100	4.33 ± 0.48	10.67 ± 0.39	3.88 ± 0.38	3.92 ± 0.37	5.93 ± 0.24	0.93 ± 0.15	1.52 ± 0.2	12.18 ± 0.25		56.64 ± 1.14
C2-EO0	4.7 ± 0.21	11.1 ± 0.37	4.42 ± 0.23	2.48 ± 0.13	5.29 ± 0.18	0.91 ± 0.09	1.15 ± 0.18	11.38 ± 0.13		58.58 ± 0.97
C2-EO2	4.11 ± 0.18	12.35 ± 0.4	3.9 ± 0.18	3.48 ± 0.17	5.85 ± 0.15	1.39 ± 0.07	1.27 ± 0.16	12.94 ± 0.13		54.72 ± 0.78
C2-EO20	4.67 ± 0.17	11.52 ± 0.36	5.82 ± 0.17	3.24 ± 0.16	4.79 ± 0.18	0.98 ± 0.07	1.5 ± 0.16	11.56 ± 0.16		55.92 ± 0.7
C2-EO100	4.06 ± 0.17	10.77 ± 0.38	2.87 ± 0.15	2.95 ± 0.14	6.29 ± 0.15	1.16 ± 0.08	1.49 ± 0.21	12.91 ± 0.19		57.5 ± 0.63
C4-EO0	3.97 ± 0.27	11.72 ± 0.61	3.14 ± 0.25	2.69 ± 0.11	5.63 ± 0.21	1.11 ± 0.07	1.13 ± 0.15	11.93 ± 0.21		58.67 ± 0.95
C4-EO2	3.16 ± 0.17	10.69 ± 0.19	3.4 ± 0.29	3.54 ± 0.12	6.26 ± 0.13	1.07 ± 0.06	1.6 ± 0.16	12.89 ± 0.1		57.38 ± 0.62
C4-EO20	4.07 ± 0.25	11.49 ± 0.35	2.86 ± 0.13	3.27 ± 0.14	6.02 ± 0.19	1.33 ± 0.08	1.36 ± 0.2	13.69 ± 0.1		55.92 ± 0.62
C4-EO100	3.39 ± 0.33	11.05 ± 0.22	3.63 ± 0.14	3.32 ± 0.18	6.15 ± 0.21	0.97 ± 0.08	1.36 ± 0.21	13.12 ± 0.15		57. ± 0.85
C8-EO0	4.4 ± 0.38	12.81 ± 0.27	3.35 ± 0.24	2.75 ± 0.16	6.45 ± 0.21	1.14 ± 0.08	1.06 ± 0.19	12.21 ± 0.11		55.83 ± 0.81
C8-EO2	3.57 ± 0.24	11.83 ± 0.27	2.77 ± 0.12	3.59 ± 0.15	6.02 ± 0.19	1.2 ± 0.08	1.22 ± 0.19	13.46 ± 0.21		56.34 ± 0.86
C8-EO20	4.18 ± 0.21	11.98 ± 0.21	3.79 ± 0.34	3.09 ± 0.21	5.07 ± 0.33	1.5 ± 0.11	1.46 ± 0.18	12.8 ± 0.27		56.13 ± 0.59
C8-EO100	4.11 ± 0.19	11.58 ± 0.22	3.21 ± 0.21	3.43 ± 0.13	6.39 ± 0.2	1.26 ± 0.08	1.38 ± 0.18	13.25 ± 0.12		55.39 ± 0.54

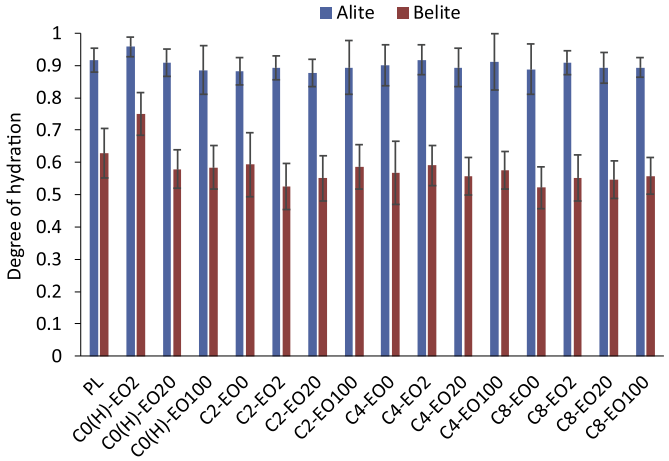

Fig. 2. Degree of hydration of alite and belite in 28-day sealed-cured pastes.

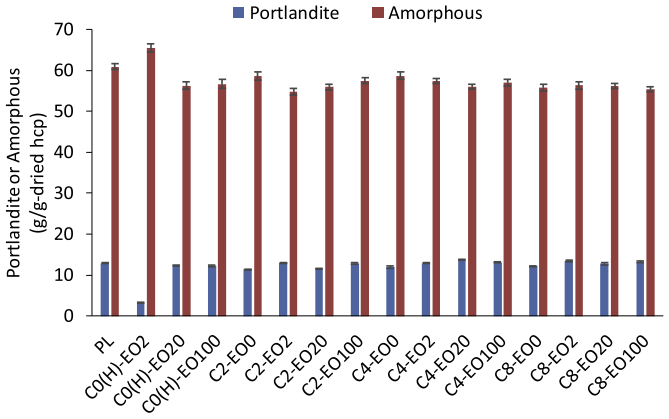

Fig. 3. Concentration of portlandite (CH) and amorphous phase in 28-day sealed-cured pastes.

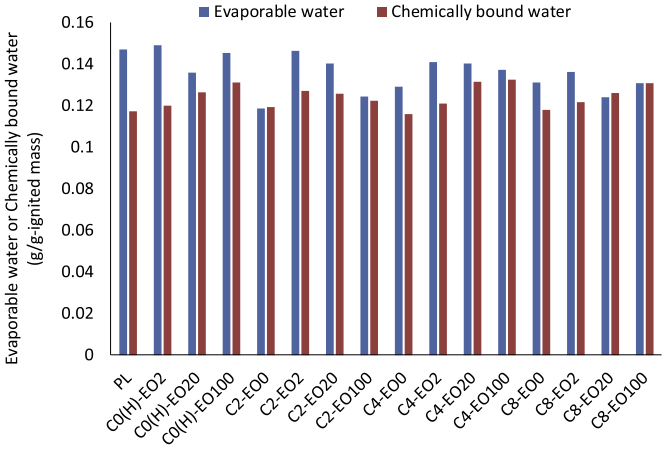

Fig. 4. Evaporable water and chemically bound water in 28-day sealed-cured pastes.

AEOP reacting with portlandite to form calcium carbonate [31,33]. Consequently, a mass loss of chemically bound water is measured between 105 °C to 550 °C. In general, both the evaporable water and the chemically bound water are not much affected by the type of AEOP. The evaporable water is slightly affected by amount of EO in the AEOP molecule and surface tension (shown in Fig. 1). The chemically bound water is slightly affected by the amount of EO in AEOP, and a larger EO content showed higher chemically bound water.

The WVSI results are shown in Fig. 6. Pretreatment was needed to measure WVSI using a volumetric method. The pretreatment involved drying under vacuum at 105 °C for 30 min. While these conditions may seem too harsh, as discussed above the AEOP cannot be affected by these pretreatment conditions. With regard to hcp, the effect is largely on the ettringite. Due to this, a larger hysteresis in the low-RH region is found using this pre-treatment. But for others, the general trend is reproduced when the data is compared with data from samples that are pre-dried at room temperature (see supplemental material). It is also questionable whether the AEOP exists in the sample even after pretreatment or not. To confirm the presence of AEOP after pre-treatment, the amount of carbon in the sample before and after treatment was measured. In all cases, the carbon mass showed little variation before and after pre-treatment. However, with regards to the total carbon amount, it is possible that grinding or other process conditions may have an impact on the number of the AEOP molecules in the samples with ethanol, methanol, butanol, octanol, and the DEG. Other than these samples, the AEOP was left. The data is shown in the supplemental material.

Finally, the difference between the data from the first desorption and this WVSI is discussed. In our previous measurement [34], a large difference was found between the first desorption and WVSI result, and capillary condensation does not seem to occur during the WVSI measurement. When the measured data is evaluated by t-plot [35] (The data of PL is shown in the supplemental material.), whose function for statistical thickness is based on the results from Badmann, Stockhausen and Setzer [36], the plot shows all the adsorption is confined in the pores and no capillary condensation occurs (Example is shown in the

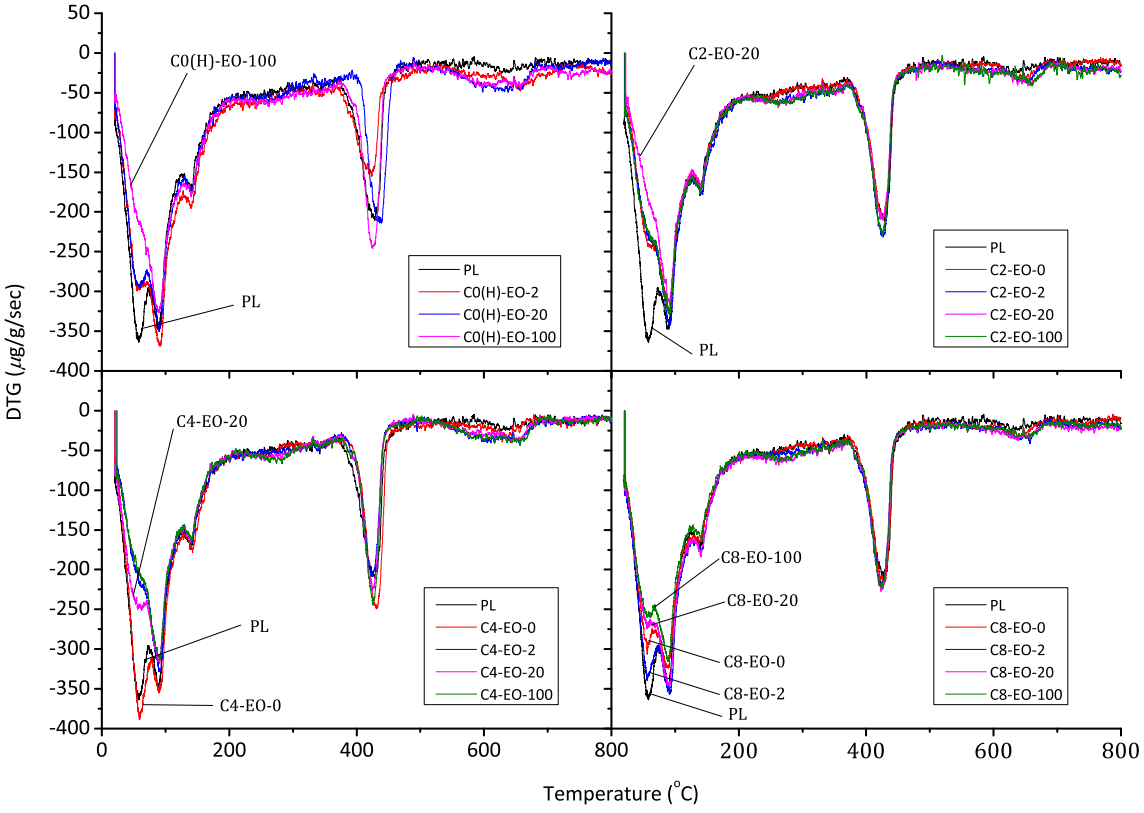

Fig. 5. DTG curves of hcp samples.

supplemental material.) Therefore, during the measurement, the impact of the liquid-gas interface is smaller than that in the first desorption. Consequently, the measurement is mainly interpreted as the behavior of water molecules in the pore-system containing AEOP.

The WVSI data were categorized based on the shapes of the isotherms. The WVSI of the plain paste shows a kink in the desorption branch at around 40% RH, which is typical of desorption isotherms of hydrated cement pastes, and it becomes stronger when the WVSI is measured rapidly.

A sudden drop in the desorption branch at around 40% RH was discussed previously [37,38], and this kink is caused by a kind of ink-bottle effect [37,39]; it is likely the kink around this RH for the case of water vapor sorption is explained by cavitation because a similar behavior is confirmed in some zeolites [40]. Cavitation is caused by nucleation of gas in the confined liquid phase with sudden evaporation from necking pores with a diameter less than the threshold value.

All of the simple alcohol samples gave similar results, with the kink close to 40% RH and little impact on the shape of the desorption isotherm. This is explained by the fact that the sample contains no alcohol. However, the ethoxylated molecules showed very different behavior. When two EOs are added to an ethyl group, the kink is shifted to higher RH values in desorption branch. When a large number of EO groups are added to either the water or small-alkyl-group-based molecules, the kink becomes weaker; in the case of C0(H)-EO-20, C0(H)-EO-100, C2-EO-20, C2-EO-100, C4-EO-20, and C4-EO-100, no clear kink are observed in desorption branch. This indicates that the microstructure of those samples does not contain a necking pore, which causes cavitation. In other words, even though they have mesopores connecting to the necking pore, the diameter of the necking pore is larger than the threshold value.

For samples other than those described above, they showed the kink at a higher RH (around 70% RH). There are two simple hypotheses that might explain this observation. One is based on the ink-bottle effect. In this case, the microstructure is changed by addition of AEOP, and necking pores with the uniform diameter are created that connect to meso-pores. The water is evaporated rapidly corresponding to the uniform necking pore diameter. The other hypothesis is that the stability of liquid water confined in meso-pores is changed due to the presence of AEOP molecules, and the relative pressure for cavitation is changed. From the viewpoint of the randomness and fractal nature of pore-structures of cement paste [41,42], the former hypothesis is not realistic. For a better understanding, the same zeolite is applied as was used in reference [40], and the SRA impact on water vapor sorption is confirmed. The result elucidates that the relative pressure for cavitation is changed by the presence of C4-EO2. The data is shown in Fig. 7.

It should be noted that the samples showing a higher kink contain AEOP with a better hydrophilic-lipophilic (HL-) balance (such as C4-EO-2, C8-EO-20, and C8-EO-100). Interestingly, this balanced condition for AEOP correlates with the lowest drying shrinkages, as shown clearly in Table 7 (detail will be discussed in Section 3.2), which takes the 8-week unrestrained drying shrinkage data (summarized in Fig. 9, which will be discussed in Section 3.2) and classifies them in the same way as in the table inset in Fig. 6.

The DSC scans of the hcp samples during freezing are shown in Fig. 8. In general, 3 peaks were observed during the cooling process. The one at around −18 °C is generally considered to be the supercooled freezing point of bulk water in large (capillary) pores. The other peaks, at around −25 °C and around −42 °C, probably correspond to the freezing points of water confined in two different classes of very small pores; the former are gel and capillary pores that are completely surrounded by the necking pores with gel pore size [43], and the latter corresponds to the homogenous ice nucleation in gel-like smaller pores [43–45]. It is believed that the strongly-adsorbed “interlayer” water does not freeze even at −42 °C [46–49], and in this measurement, at most only 20% of evaporable water was frozen. In general, the area under the peak at −42 °C, which is summarized in Table 6, is reduced by long-chain EO polymers and also by DEG, but not by aliphatic alcohols or the more strongly hydrophobic AEOP molecules (e.g. C8-EO-

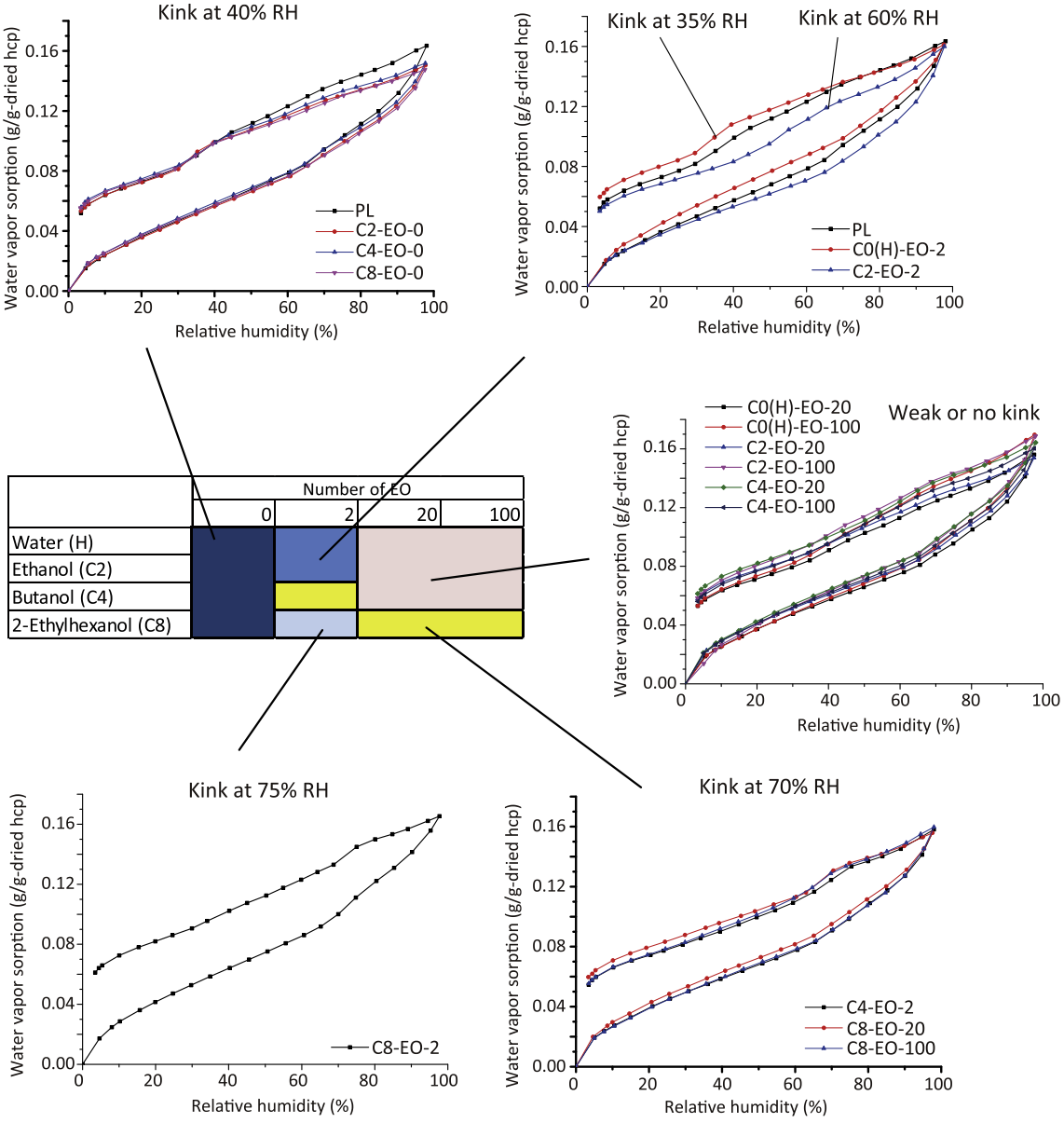

Fig. 6. Classification of the main AEOP groups with respect to their influence on the water vapor sorption isotherms of hardened cement paste (especially the kink in the desorption branch).

2). Similar trends of matured hcp containing SRA were observed in previous studies [8,43]. In those papers, the impact of SRA on LTC measurement is discussed. Generally, SRA has an impact on depression of the freezing temperature, while Bentz [8] concluded that the freezing point depressions are significantly reduced in the case of hcp containing SRA by the reduced liquid-gas and/or liquid-ice surface tensions of the pore solution. In addition, SRA molecules serve as ice nucleation agents. The impact of this role is seen when cement paste is at an early age and has a large connectivity of pores [8,43]. According to Fig. 8, the AEOP with the better HL-balance showed a shift to lower temperature and a reduction of the peak at around −42 °C. Based on the previous studies mentioned above, the depression of freezing temperature is evidence that the SRA, which is arranged on the surface of pore-walls [43] (because there exists a strong interaction between hydration products and organic molecules, such as polyethylene glycols [50]), interacts with pore solution and depresses the freezing temperature. Reduction of the peak at around −42 °C can be explained by two hypotheses. The first hypothesis proposes it is due to the role of SRA in ice nucleation in capillary pores at higher temperature, which consumes the water supplied from the smaller pores and resultantly, the peak is reduced. The second hypothesis proposes it is due to pre-structuring of water by self-assembly of SRA molecules located on the pore-walls.

3.2. Deformation and mass change

Long-term shrinkage strains of hcp samples after drying at 60% RH for 8 weeks are shown in Fig. 9, and the results are also classified as a function of AEOP structure in Table 7 for ease of comparison. C4-EO-2 and C8-EO-20 gave the best shrinkage reductions, at only about half the shrinkage strain of PL. Only the sample made with DEG (C0(H)-EO-2) showed an increase in drying shrinkage strain, which was very significant (about 20% more shrinkage than PL). This can probably be explained by the significantly larger amorphous phase (i.e. C-S-H) and smaller amount of crystalline portlandite in this hcp, although the C-S-H structure itself may also be significantly modified. The simple alcohols gave the largest shrinkages for each series (C0(H), C2, C4, and C8), and there seemed to be an optimum balance between the size of the alkyl group and the length of the poly-EO chain for minimal shrinkage

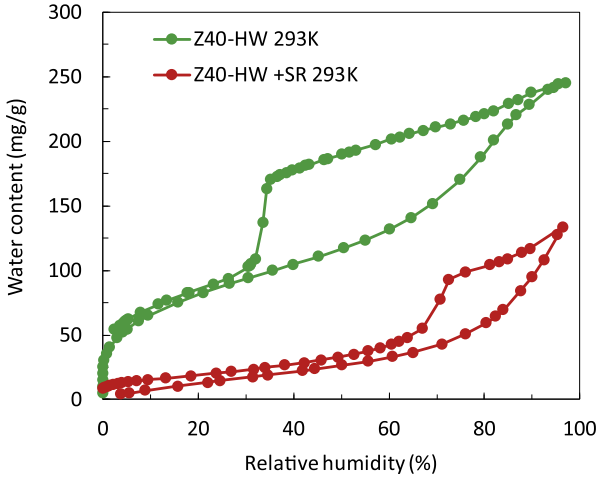

Fig. 7. Comparison of water sorption isotherms of zeolite Z40-HW (according to ref. [40]) with/without C4-EO2. The applied pretreatment method was the same as that for the data shown in Fig. 6.

in each series. In the C2 and C4 series, EO-2 gave the best shrinkage reduction; in the C8 series, C8-EO-20 showed the best shrinkage reduction.

Fig. 10 shows the mass losses of the hcp samples after 8 weeks of drying. The results can be classified into three groups. PL, C0(H)-EO-20, C0(H)-EO-100, C4-EO-2, and C8-EO-100 form the group with the largest mass losses, with C4-EO-2 giving the largest value. The minimum mass loss group contains C0(H)-EO-2, C2-EO-0, C4-EO-0, C4-EO-20, and C8-EO-0.

Table 6
Area under DSC peak around −42 °C (mJ/cm^3-hcp).

	Number of EO			
	0	2	20	100
Water (H)	0.0241	0.0118	0.0114	0.0166
Ethanol (C2)	0.0287	0.0067	0.0062	0.0133
Butanol (C4)	0.03	0.0033	0.0054	0.0051
2-Ethylhexanol (C8)	0.0248	0.03	0.0055	0.0057

Although there is a lot of scatter, the samples with smaller drying mass losses tended to show greater drying shrinkage (Fig. 11). This might be explained, as shown in Fig. 12, by the hypothesis that the amount of amorphous phase in hcp is the dominant factor with regard to shrinkage strain [51].

The short-term length change data are summarized in Fig. 13. Short-term shrinkage behavior correlates well with long-term shrinkage behavior, as shown in Fig. 14. The sample with DEG gave the largest shrinkage, and the samples with C4-EO-2, C2-EO-2, and C8-EO-20 gave the lowest shrinkage. As shown in Fig. 15, the main reduction effect of AEOPs on short-term shrinkage occurred between about 75% and 40% RH, in agreement with previous observations [12,13]. In this figure, incremental strain from 90% RH to 75% RH (blue bars) and 40% RH to 20% RH (gray bars) were nearly identical among all samples. Consequently, the shrinkage performance can be evaluated by the

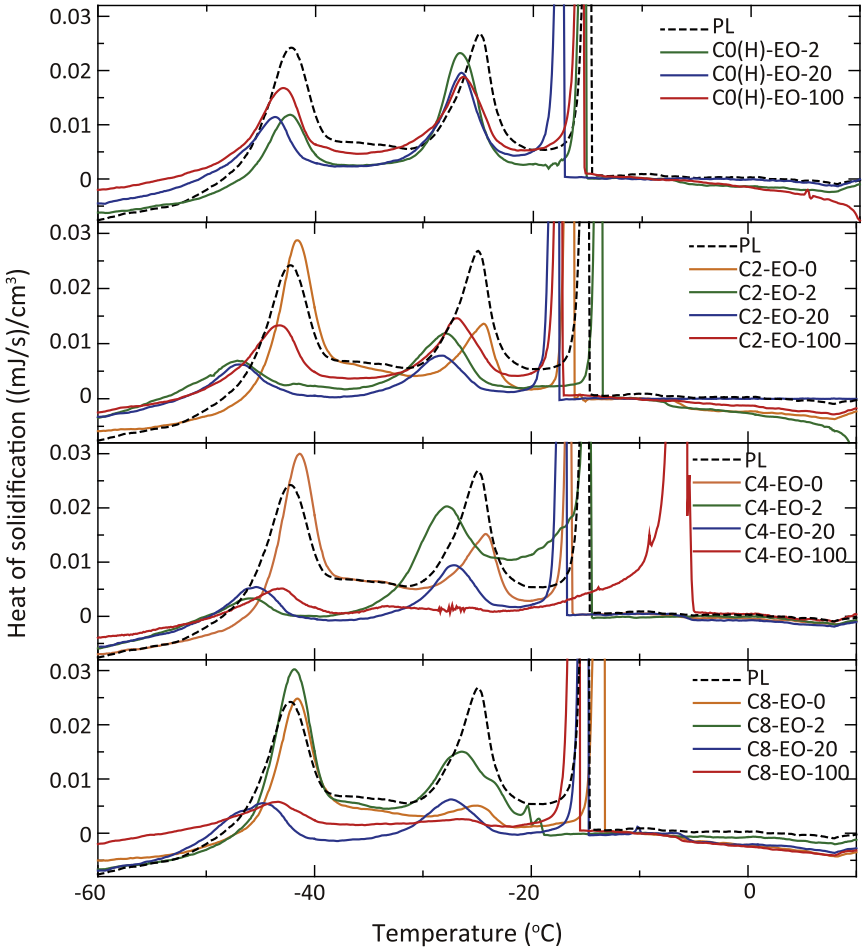

Fig. 8. DSC trace of the first cooling of hcp samples with AEOP or without (PL).

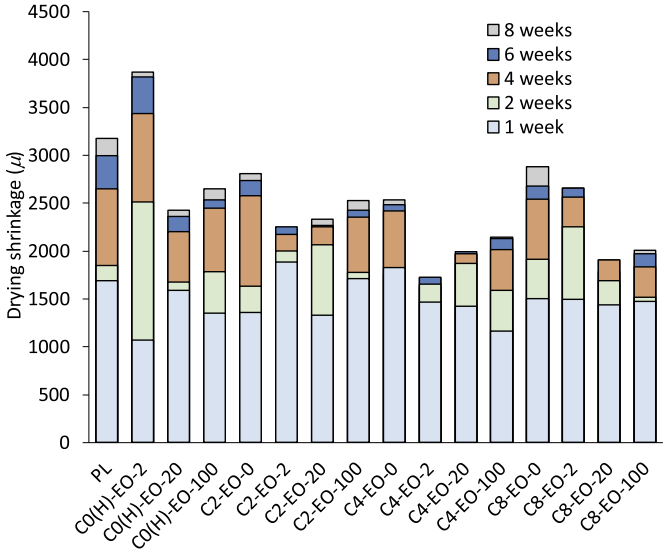

Fig. 9. 8-week drying shrinkage strains of hcp with AEOP, or without (PL).

Table 7
Classification of 8-week shrinkage strains of hcp as a function of AEOP composition. (Unit: μ).

	Number of EO			
	0	2	20	100
Water (H)	3177	3867	2428	2650
Ethanol (C2)	2808	2233	2335	2529
Butanol (C4)	2534	1717	1968	2149
2-Ethylhexanol (C8)	2879	2659	1783	2006

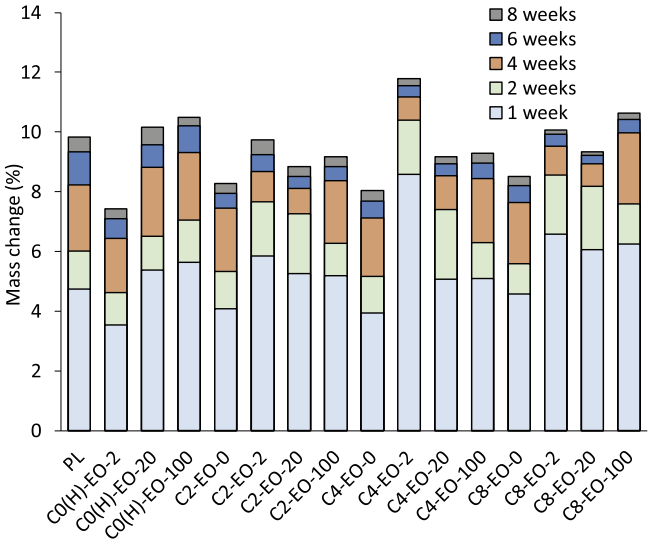

Fig. 10. Mass losses over 8-week drying for hcp samples with AEOP, or without (PL).

incremental strain from 75% RH to 40% RH (orange bars), in which AEOPs play a significant role in hcp [5,12,13]. It was also confirmed that the expansive strain during re-humidification is almost unaffected by the presence of AEOPs. The incremental strains in the re-humidification (adsorption) process are summarized in Fig. 16. Incremental strain during the re-humidification process under each RH region showed similar values.

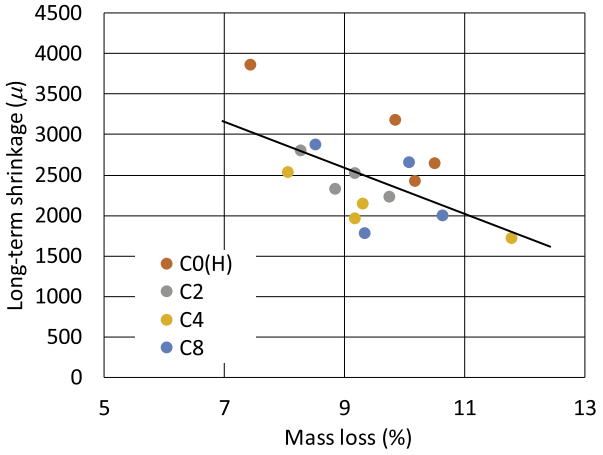

Fig. 11. Relationship between mass loss and long-term shrinkage of hcp.

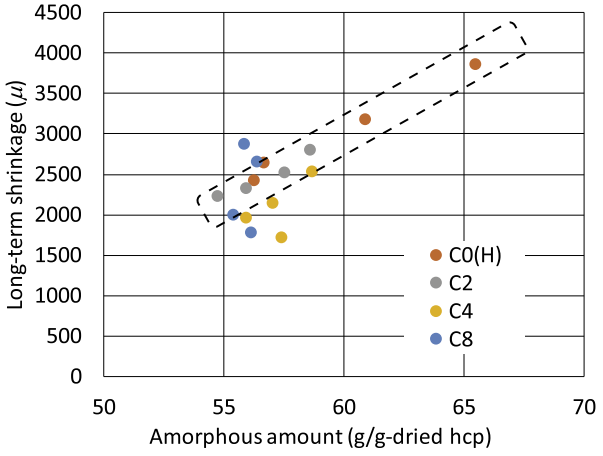

Fig. 12. Relationship between amount of amorphous phase and long-term shrinkage of hcp.

4. Discussion

Based on the data shown in Fig. 13, the differences in incremental strain of three RH regions, i.e. 90–75, 75–40, and 75–20% RH, were evaluated and the results are shown in Fig. 17. It has been confirmed that mainly irreversible shrinkage occurs from 75% RH to 40% RH, and this irreversible shrinkage strain is affected by the addition of AEOP. In other words, the main goal of reducing drying shrinkage is attained by restraining irreversible shrinkage, as suggested in previous research [13]. In reference [13], the hypothesis was proposed that the change in irreversible shrinkage strain is caused by the change in the crystal size of Portlandite by the adsorption of SRA on its surfaces.

However, looking into the drying region from 75% RH to 40% RH, readers may notice a new mechanism. As the LTC showed, the addition of AEOP has an influence on the heat of solidification at around −42 °C and the peak shift. Fig. 18 shows the relationship between the heat of solidification at around −42 °C and long-term shrinkage strain at 60% RH. It can be seen that the solidification heat gives a good positive correlation with shrinkage strain; however, the sample containing DEG is clearly anomalous. This can perhaps be explained by its much larger content of “amorphous” C-S-H, the main phase responsible for the shrinkage of hcp (as suggested by the results shown in Fig. 12).

To better understand the effects of solidification at about −42 °C, the results of supplementary LTC measurements on white Portland hcp samples, which were slowly dried under different RHs for 1 year (as discussed in refs. [27, 28, 38]) are shown in Fig. 19. The trend of the experimental results is consistent with previous results [52–55].

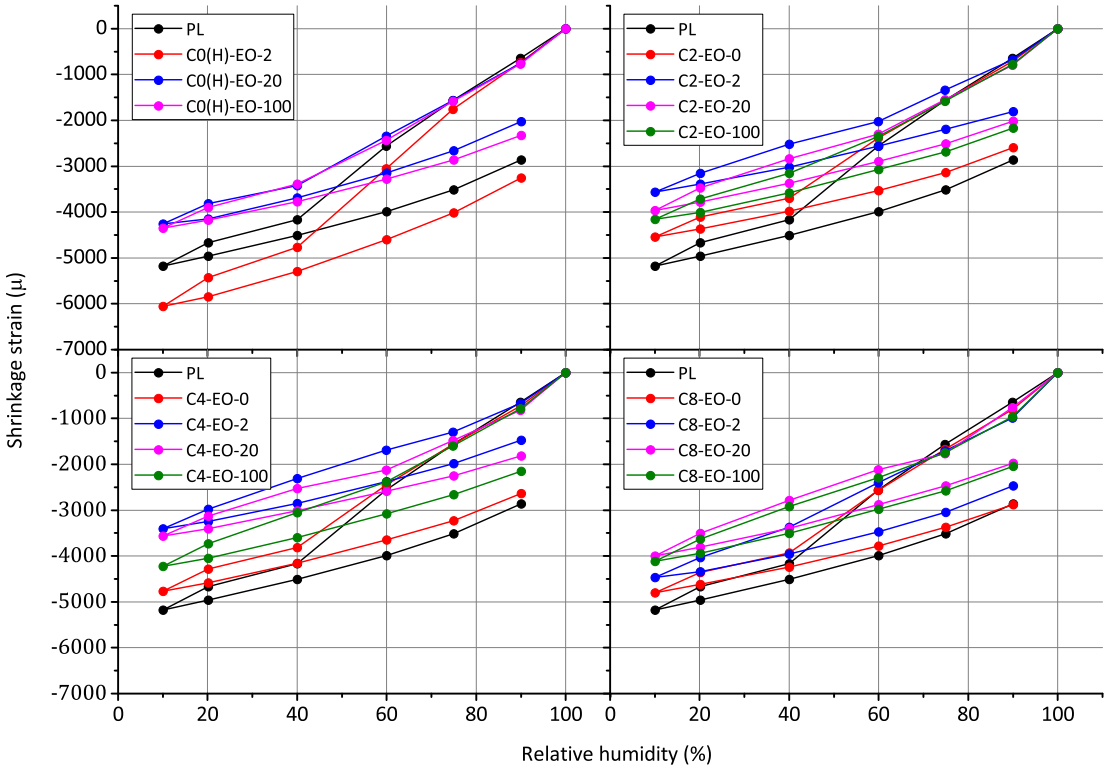

Fig. 13. Short-term length change isotherms of hcp samples without (PL) and with AEOP.

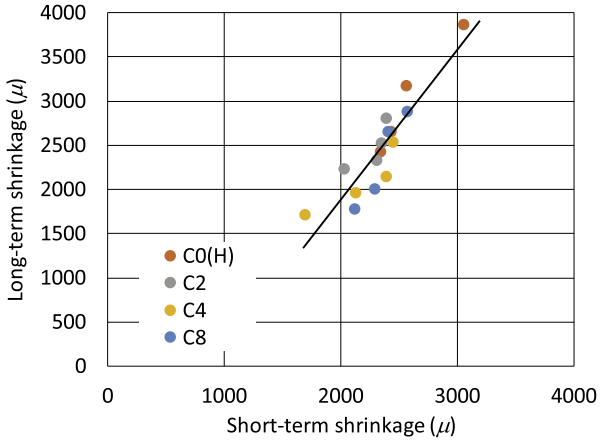

Fig. 14. Comparison of long-term and short-term shrinkage strains at 60% RH.

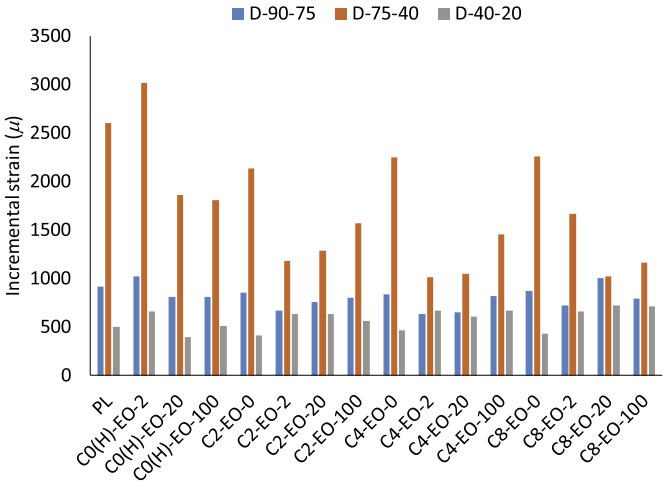

Fig. 15. Incremental strains from 90% RH to 75% RH (D-90-75), from 75% RH to 40% RH (D-75-40), and from 40% RH to 10% RH (D-40-20) of short-term length change isotherms during the first drying.

Samples dried at 80% RH or more (80, 90, and 100% RH) show complex exothermic peaks above −35 °C, while samples dried at or below 70% RH (70, 60, 50, and 40% RH) show a sole peak at around −42 °C, and the area under this peak decreases with decreasing sample RH. Therefore, the heat of solidification at around −42 °C is strongly related to drying in the region from 75% to 40% RH. As previously discussed, the peak shift and probably the reduction of the heat of solidification are evidence of the presence of SRA in the relevant microstructure. This microstructure corresponds to the pores where the water evaporates from 75% RH to 40% RH.

With regard to the WVSI, the kink position is shifted to higher RHs by the better HL-balanced AEOP. This kink is considered to be related to cavitation (currently this is a hypothesis based on reference [40], but if the phenomenon is explained by the ink-bottle effect, the discussion is still applicable) of confined solution in the pores, which almost corresponds to the pores related to the heat of solidification at around −42 °C. The relative pressure for cavitation is determined by the liquid-vapor surface tension [56–58]. Ion and surfactant concentrations have an impact on the threshold vapor pressure (related to measured RH) for causing cavitation [59,60]. Also, it has been reported that surfactants may increase the threshold vapor pressure by attaining a critical concentration in the pore solution, and the radius of nucleus/meniscus is changed by the number of molecules at liquid-gas interfaces [60]. This scenario agrees with the sorption model for hcp containing SRA developed by Eberhardt [12].

It should be recalled that drying in the region from 75% RH to 40% RH does not only empty the pores but does change the microstructure, especially in the case of long-term drying. For example, Fig. 20 shows that the water vapor sorption isotherms change dramatically after long-term drying under different RH conditions, and the changes indicate a

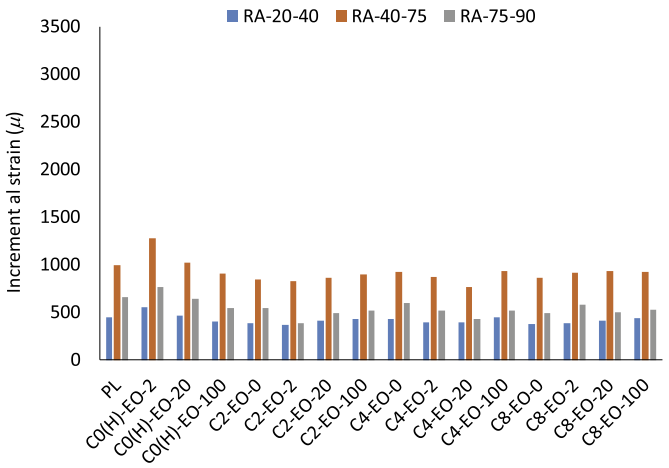

Fig. 16. Incremental strain from 90% RH to 75% RH (RA-90-75), 75% RH to 40% RH (RA -75-40), and 40% RH to 10% RH (RA -40-20) length change isotherms during the re-humidification process.

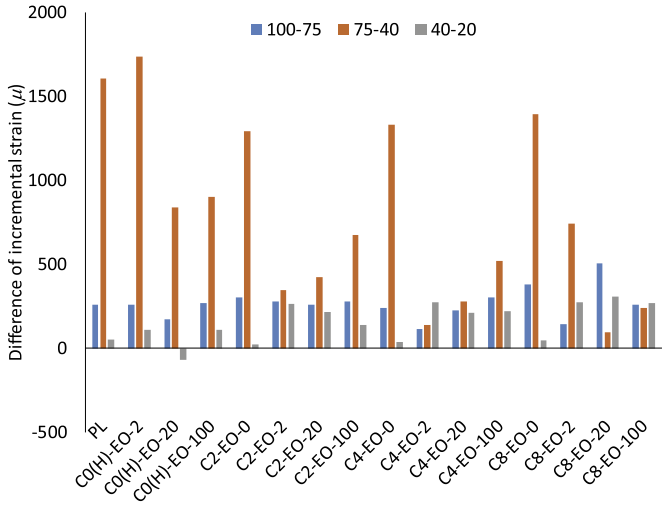

Fig. 17. Difference of incremental strain of the first desorption and re-humidifying process in three RH regions: 90–75, 75–40, and 40–20% RH.

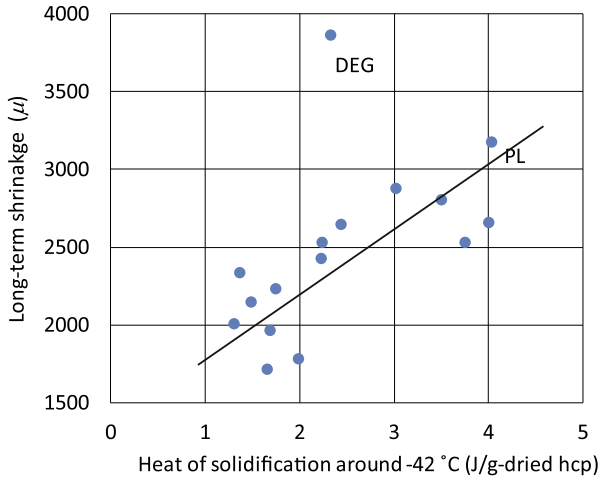

Fig. 18. Long-term shrinkage strain at 60% RH vs. heat release around −42 °C for hcp samples made with AEOP or without (PL).

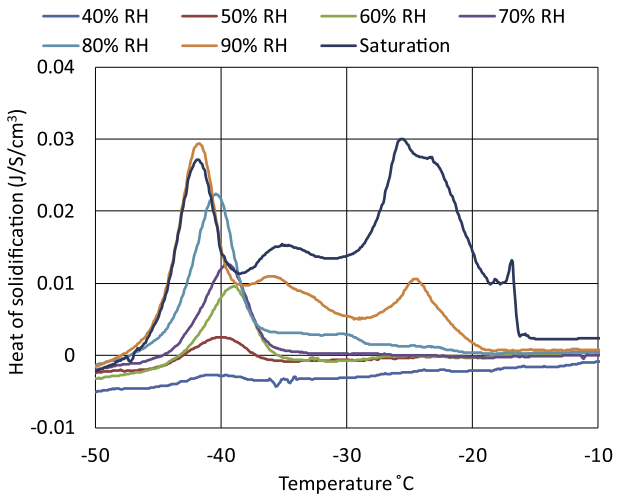

Fig. 19. Low temperature DSC scans of mature white Portland cement paste samples slowly-dried at different relative humidities. The measurement procedures were the same as those used for the data in Fig. 8.

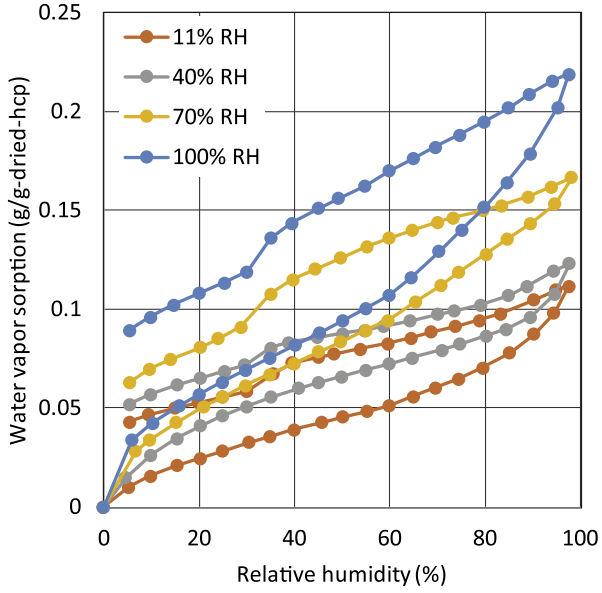

Fig. 20. Water vapor sorption isotherms of mature white Portland cement paste samples slowly dried at different relative humidities [61].

decrease in meso-pores, which absorb water above 40% RH. Resultingly, both LTC and WVSI measurements suggested that the SRA molecules exist in the pores where the water evaporates from 75% RH to 40% RH, and these SRA molecules mitigate the agglomeration of C-S-H sheets during the first drying [28,38], which cause irreversible shrinkage as confirmed by Fig. 17.

When we try to interpret irreversible shrinkage in terms of GMC theory, we must first remember that the total bulk irreversible shrinkage of cement paste only represents a small fraction of the total volume of water lost, because much of the lost water volume simply goes into forming empty porosity. This porosity exists in part because of the random orientation of sheets and platelets or "packets" of platelets of C-S-H, and partly because of the formation of "bubble-like" gel pores between sheets. The NMR evidence seems to imply that the gel pores form even before drying starts [23], so much of the irreversible bonding presumably occurs at "out-of-plane" contact points between such packets of platelets, which become bonded together by permanent ≡Si−O−Ca−O−Si≡linkages. However, the transverse spacing

between the parallel sheets within packets must have a considerable influence on hysteresis in the water vapor isotherms, as exemplified by the "kinks" observed. If, as seems likely, AEOP molecules with several EO groups can be arranged on the pore walls [43] or free C-S-H basal surfaces [50], they could potentially take up some of the space that would otherwise be taken up by gel water and/or by water ligands around charge-balancing calcium ions. We do not believe that all of the water freezes at −42 °C, but we can assume that the water that freezes at −42 °C must be in very small pores in close proximity to C-S-H surfaces upon which such AEOPs could presumably become arranged.

Some of these AEOPs may also become trapped in gel pores, which could give them the appearance of being adsorbed in an "immobile" form, as confirmed by Eberhardt [12]. They are also likely to limit the formation of permanent ≡Si−O−Ca−O−Si≡bonds between "packets" or "agglomerates" of sheets, and this is presumably what explains most of their beneficial effect, i.e. reduced irreversible shrinkage. Therefore, the "immobile SRA" reported by Eberhardt [12] could well correlate with better SRA performance in irreversible drying shrinkage between 75% and 40% RH.

Based on the classical disjoining pressure theory in hardened cement paste, other interpretations are possible. With respect to disjoining pressure theory, irreversible shrinkage is explained by narrowing of C-S-H sheets under drying, yielding multiple energetic minima for surfaces in close vicinity under shear superposition due to attractive and repulsive forces in the packet of C-S-H sheets. Consequently, re-organization of packets of C-S-H sheets is possible during the first drying, and the presence of AEOPs in the vicinity of the C-S-H sheets alters the condition for the multiple energetic minima and reduces the stability after the re-organization of packets of C-S-H sheets. In summary, the presence of AEOP near C-S-H sheets has an important role on the irreversible drying-induced organization. This discussion is in line with the proposed perspective of SRA mechanism by Eberhardt [12].

From the viewpoint of classical capillary tension theory, SRA has an effect on gas-liquid interfaces, as confirmed by Eberhardt [12]. However, the impact on shrinkage during the first desorption is likely to be small, say several hundred microns of shrinkage, because reversible shrinkage of hcp is very small [12,13]. As for the previous mechanism, that SRA is adsorbed on the surface of portlandite and produces fine portlandite crystals, including smaller inter-spaces, by regulating crystal growth; this role might be relevant, but in the present study the other mechanism is spotlighted.

5. Conclusions

A series of alkyl-ethylene oxide polymers (AEOPs) synthesized with controlled variations of their main structural elements was investigated by a wide range of techniques to determine their effect on the drying behavior of well-hydrated white cement pastes. The following conclusions have been reached:

1) AEOPs can subtly change the shape of water vapor sorption isotherms, displacing the kink in the desorption branch from around 35% RH (for DEG) and 40% RH (for the plain paste) up to about 75% RH in the extreme case. Displacement of the kink to higher RH roughly correlates with a greater degree of shrinkage reduction, with an optimum at about 70% RH. This mechanism might be explained by the increase of critical vapor pressure due to the presence of better hydrophilic-lipophilic balance AEOPs in mesopores connecting to necking pores causing cavitation. This apparent optimal kink position corresponds with the use of the two most effective shrinkage-reducing AEOP molecules, C4-EO-2 and C8-EO-20, both of which gave only about half the drying shrinkage of the control paste. These molecules apparently have the best balance between the hydrophobic alkyl group and the hydrophilic poly-EO chain.
2) Addition of effective shrinkage-reducing AEOPs also significantly reduces the peak for the heat of water solidification at around −42 °C in the cooling branch of low temperature DSC scans. The drying shrinkage of the hcps decreases roughly with decreasing area under this peak, even though the mechanism of the reduction of the solidification peak is not clarified, but the peak temperature shift is evidence of the presence of AEOP in the corresponding meso-pores.
3) Based on the temperature peak shift at −42 °C in the cooling branch of low temperature DSC scans, the relative humidity shift of sudden drop in the water vapor sorption isotherm suggest the presence of SRA in the corresponding meso-pores in which the water molecules evaporate from 75% RH to 40% RH. Short-term length change isotherms show that even the most effective AEOPs mainly reduce only the largely irreversible shrinkage that occurs during the first desorption, from 75% down to 40% RH. Based on the corresponding RH region in low temperature DSC scans, water vapor sorption isotherms, and irreversible shrinkage shown by the short-term length change isotherms, it is concluded that the better hydrophilic-lipophilic balance AEOPs exist in the meso-pores, and they mitigate the irreversible shrinkage by keeping the C-S-H sheets apart, which generally agglomerate under the first drying.

Acknowledgement

One of the authors, Dr. Ellis Martin Gartner, sadly passed away on the 13th of February 2018. The other authors thank him for his inspiring discussions. The authors would also like to express our sincere gratitude to the anonymous reviewer who contributed to this paper through constructive comments. The water vapor sorption of zeolite was conducted by Jiří Rymeš (Ph.D. student, Nagoya University, collaborative research with Chubu Electric Power Co., Inc.). Dr. Matthieu Vandamme (Ecole des Ponts ParisTech - Laboratoire Navier) and Prof. Benoit Coasne (University Grenoble Alpes) are acknowledged for discussions on the kink of water vapor sorption isotherms.

Appendix A. Supplementary data

Supplementary data to this article can be found online at https://doi.org/10.1016/j.cemconres.2018.05.017.

References

[1] T. Goto, T. Sato, K. Sakai, Cement Shrinkage Reducing Agent and Cement Composition, United States Patent and Trademark Office, United States, 1985www.uspto.gov.
[2] T. Sato, T. Goto, K. Sakai, Mechanism for reducing drying shrinkage of hardened cement by organic additives, CAJ Rev. (1983) 52–54.
[3] M. Sakuta, T. Saitou, S. Oono, H. Kasami, Utilization of shrinkage reducer to construction of reinforced concrete walls: part II mechanism of shrinkage reduction (in Japanese), Summaries of Technical Papers of Annual Meeting of Architectural Institute of Japan, Structure, 59 1984, pp. 489–490.
[4] K. Saito, K. Inoue, M. Kinoshita, H. Shiigai, R. Kobayashi, K. Mitsui, Study on 200 μ class super-low drying-shrinkage concrete with frost damage resistance, Summaries of Technical Papers of Annual Meeting of Architectural Institute of Japan 2012 (2012) 735–736 (1368).
[5] J. Weiss, P. Lura, F. Rajabipour, G. Sant, Performance of shrinkage-reducing admixtures at different humidities and at early ages, ACI Mater. J. 105 (2008) 478–786.
[6] D.P. Bentz, M.R. Geiker, K.K. Hansen, Shrinkage-reducing admixtures and early-age desiccation in cement pastes and mortars, Cem. Concr. Res. 31 (2001) 1075–1085.
[7] C. Maltese, C. Pistolesi, A. Lolli, A. Bravo, T. Cerulli, D. Salvioni, Combined effect of expansive and shrinkage reducing admixtures to obtain stable and durable mortars, Cem. Concr. Res. 35 (2005) 2244–2251.
[8] D.P. Bentz, Influence of shrinkage-reducing admixtures on early-age properties of cement pastes, J. Adv. Concr. Technol. 4 (2006) 423–429.
[9] A. Rubeurim, A. Carrajola, A. Goncalves, F. Branco, Effectiveness of shrinkage reducing admixtures on cracking of mortar specimens, RILEM-JCI Seminar on Concrete Durability and Service Life Plannning, ConreteLife'06, RILEM, Ein-Bokek, Dead Sea, Israel, 2006, pp. 214–224.
[10] P. Lura, B. Pease, G.B. Mazzotta, F. Rajabipour, J. Weiss, Influence of shrinkage-reducing admixtures on development of plastic shrinkage cracks, ACI Mater. J. 104 (2007) 187–194.
[11] F. Rajabipour, G. Sant, J. Weiss, Interactions between shrinkage reducing admixtures (SRA) and cement paste's pore solution, Cem. Concr. Res. 38 (2008)

606–615.
[12] A.B. Eberhardt, On the Mechanisms of Shrinkage Reducing Admixtures in Self-consolidating Mortars and Concretes, Shaker Verlag GmbH, Aachen, 978-3-8440-0027-6, 2009.
[13] I. Maruyama, K. Beppu, R. Kurihara, A. Furuta, Action mechanisms of shrinkage reducing admixture in hardened cement paste, J. Adv. Concr. Technol. 14 (2016) 311–323.
[14] K. Nakayama, T. Shouji, K. Makino, Influence of alcohol on the specific surface area of slaked lime powder generated from quicklime, Journal of the Association of Materials Engineering for Resources 13 (2000) 82–87.
[15] Y. Kojima, S. Hirose, Y. Tomita, Effect of additive on crystal shape and particle size of calcium hydroxide, Journal of the Society of Inorganic Materials, Japan 22 (2015) 255–260.
[16] J.J. Thomas, J.J. Chen, H.M. Jennings, D.A. Neumann, Ca – OH bonding in the C – S – H gel phase of tricalcium silicate and white Portland cement pastes measured by inelastic neutron scattering, Chem. Mater. 15 (2003) 3813–3817.
[17] I.G. Richardson, Tobermorite/jennite- and tobermorite/calcium hydroxide-based models for the structure of C-S-H: applicability to hardened pastes of tricalcium silicate, β-dicalcium silicate, Portland cement, and blends of Portland cement with blast-furnace slag, metakaolin, or silica fume, Cem. Concr. Res. 34 (2004) 1733–1777.
[18] I.G. Richardson, The calcium silicate hydrates, Cem. Concr. Res. 38 (2008) 137–158.
[19] I. Richardson, Model structures for C-(A)-S-H(I), Acta Crystallographica Section B 70 (2014) 903–923.
[20] E.M. Gartner, A proposed mechanism for the growth of C-S-H during the hydration of tricalcium silicate, Cem. Concr. Res. 27 (1997) 665–672.
[21] E.M. Gartner, K.E. Kurtis, P.J.M. Monteiro, Proposed mechanism of C-S-H growth tested by soft X-ray microscopy, Cem. Concr. Res. 30 (2000) 817–822.
[22] E. Gartner, I. Maruyama, J. Chen, A new model for the C-S-H phase formed during the hydration of Portland cements, Cem. Concr. Res. 97 (2017) 95–106.
[23] J.F. Young, W. Hansen, Volume relationships for C-S-H formation based on hydration stoichiometries, MRS Proc. 85 (1986) 313–322.
[24] C. Hua, A. Ehrlacher, P. Acker, Analyses and models of the autogenous shrinkage of hardening cement paste II. Modelling at scale of hydrating grains, Cem. Concr. Res. 27 (1997) 245–258.
[25] T. Zhang, S. Shang, F. Yin, A. Aishah, A. Salmiah, T.L. Ooi, Adsorptive behavior of surfactants on surface of Portland cement, Cem. Concr. Res. 31 (2001) 1009–1015.
[26] F. Merlin, H. Guitouni, H. Mouhoubi, S. Mariot, F. Vallée, H. Van Damme, Adsorption and heterocoagulation of nonionic surfactants and latex particles on cement hydrates, J. Colloid Interface Sci. 281 (2005) 1–10.
[27] I. Maruyama, Y. Nishioka, G. Igarashi, K. Matsui, Microstructural and bulk property changes in hardened cement paste during the first drying process, Cem. Concr. Res. 58 (2014) 20–34.
[28] I. Maruyama, G. Igarashi, Y. Nishioka, Bimodal behavior of C-S-H interpreted from short-term length change and water vapor sorption isotherms of hardened cement paste, Cem. Concr. Res. 73 (2015) 158–168.
[29] I. Maruyama, G. Igarashi, Cement reaction and resultant physical properties of cement paste, J. Adv. Concr. Technol. 12 (2014) 200–213.
[30] A. Jenni, L. Holzer, R. Zurbriggen, M. Herwegh, Influence of polymers on microstructure and adhesive strength of cementitious tile adhesive mortars, Cem. Concr. Res. 35 (2005) 35–50.
[31] B. Lothenbach, P. Durdzinski, K. De Weerdt, Thermogravimetric analysis, in: K. Scrivener, R. Snellings, B. Lothenbach (Eds.), A Practical Guide to Microstructural Analysis of Cementitious Materials, 2015, pp. 178–208.
[32] R. Kriegel, R. Hellrung, A. Dimmig, Qualitative and quantitative analysis of selected organic additives in hardened concrete by thermal analysis and infrared spectroscopy, Proceedings of the 11th iInternational Congress on the Chemistry of Cement, Durban, 2003, pp. 171–180.
[33] M.D.A. Thomas, The suitability of solvent exchange techniques for studying the pore structure of hardened cement paste, Adv. Cem. Res. 2 (1989) 29–34.
[34] I. Maruyama, Origin of drying shrinkage of hardened cement paste: hydration pressure, J. Adv. Concr. Technol. 8 (2010) 187–200.
[35] B.C. Lippens, B.G. Linsen, J.H.d. Boer, Studies on pore systems in catalysts I. The adsorption of nitrogen; apparatus and calculation, J. Catal. 3 (1964) 32–37.
[36] R. Badmann, N. Stockhausen, M.J. Setzer, The statistical thickness and the chemical potential of adsorbed water films, J. Colloid Interface Sci. 82 (1981) 534–542.
[37] V. Baroghel-Bouny, Water vapour sorption experiments on hardened cementitious materials: part I: essential tool for analysis of hygral behaviour and its relation to pore structure, Cem. Concr. Res. 37 (2007) 414–437.
[38] I. Maruyama, N. Sakamoto, K. Matsui, G. Igarashi, Microstructural changes in white Portland cement paste under the first drying process evaluated by WAXS, SAXS, and USAXS, Cem. Concr. Res. 91 (2016) 24–32.
[39] S. Brunauer, R.S. Mikhail, E.E. Bodor, Some remarks about capillary condensation and pore structure analysis, J. Colloid Interface Sci. 25 (1967) 353–358.
[40] M. Thommes, S. Mitchell, J. Pérez-Ramírez, Surface and pore structure assessment of hierarchical MFI zeolites by advanced water and argon sorption studies, J. Phys. Chem. C 116 (2012) 18816–18823.
[41] A.J. Allen, R.C. Oberthur, D. Pearson, P. Schofield, C.R. Wilding, Development of the fine porosity and gel structure of hydrating cement systems, Philosophical Magazine Part B 56 (1987) 263–288.
[42] A.J. Allen, J.J. Thomas, H.M. Jennings, Composition and density of nanoscale calcium-silicate-hydrate in cement, Nat. Mater. 6 (2007) 311–316.
[43] G. Sant, D. Bentz, J. Weiss, Capillary porosity depercolation in cement-based materials: measurement techniques and factors which influence their interpretation, Cem. Concr. Res. 41 (2011) 854–864.
[44] G.W. Scherer, Freezing gels, J. Non-Cryst. Solids 155 (1993) 1–25.
[45] Z. Sun, G.W. Scherer, Pore size and shape in mortar by thermoporometry, Cem. Concr. Res. 40 (2010) 740–751.
[46] M. Brun, A. Lallemand, J.-F. Quinson, C. Eyraud, A new method for the simultaneous determination of the size and shape of pores: the thermoporometry, Thermochim. Acta 21 (1977) 59–88.
[47] A.A. Antoniou, Phase transformations of water in porous glass, J. Phys. Chem. 68 (1964) 2754–2763.
[48] G.G. Litvan, Phase transitions of adsorbates: 1. Specific heat and dimensional changes of the porous glass – water system, Can. J. Chem. 44 (1966) 2617–2622.
[49] D.H. Bager, E.J. Sellevold, Ice formation in hardened cement paste, part I — room temperature cured pastes with variable moisture contents, Cem. Concr. Res. 16 (1986) 709–720.
[50] J.J. Beaudoin, H. Dramé, L. Raki, R. Alizadeh, Formation and properties of C-S-H–PEG nano-structures, Mater. Struct. 42 (2009) 1003–1014.
[51] T. Haji, S. Kotera, R. Kurihara, I. Maruyama, Impact of demolding age and mineral composition of cement on drying shrinkage of cement paste, Proceedings of Japan Concrete Instituite, 38 2016, pp. 45–50.
[52] N. Stockhausen, H. Dorner, B. Zech, M.J. Setzer, von Untersuchung, gefriervorgängen in zementstein mit hilfe der DTA, Cem. Concr. Res. 9 (1979) 783–794.
[53] D.H. Bager, E.J. Sellevold, Ice formation in hardened cement paste, part II — drying and resaturation on room temperature cured pastes, Cem. Concr. Res. 16 (1986) 835–844.
[54] R.E. Beddoe, M.J. Setzer, Phase transformations of water in hardened cement paste a low-temperature DSC investigation, Cem. Concr. Res. 20 (1990) 236–242.
[55] K.A. Snyder, D.P. Bentz, Suspended hydration and loss of freezable water in cement pastes exposed to 90% relative humidity, Cem. Concr. Res. 34 (2004) 2045–2056.
[56] R. Becker, W. Döring, Kinetische Behandlung der Keimbildung in übersättigten Dämpfen, Ann. Phys. 416 (1935) 719–752.
[57] J.C. Fisher, The fracture of liquids, J. Appl. Phys. 19 (1948) 1062–1067.
[58] E. Herbert, S. Balibar, F. Caupin, Cavitation pressure in water, Phys. Rev. E 74 (2006) 041603.
[59] F.E. Fox, K.F. Herzfeld, Gas bubbles with organic skin as cavitation nuclei, The Journal of the Acoustical Society of America 26 (1954) 984–989.
[60] A.A. Atchley, L.A. Crum, The Nucleation of Cavitation in Aqueous Media, Mississippi Univ University Physical Acoustics Research Lab, 1985.
[61] I. Maruyama, O. Kontani, M. Takizawa, S. Sawada, S. Ishikawao, J. Yasukouchi, O. Sato, J. Etoh, T. Igari, Development of soundness assessment procedure for concrete members affected by neutron and gamma-ray irradiation, J. Adv. Concr. Technol. 15 (2017) 440–523.